

Coulomb Explosion of an Electron Gas in a Uniform Magnetic Field

Omid Zandi and Renske M. van der Veen

Department of Chemistry, University of Illinois at Urbana-Champaign, Urbana, IL 61801, USA

Materials Research Laboratory, University of Illinois at Urbana-Champaign, Urbana, IL 61801, USA

Abstract- A method is developed to analyze the behavior of electron distributions under their own electric field and an external uniform magnetic field. The method is based on the derivation of the current density and hence the drift velocity from the charge-current continuity equation, which is used in either the Hamiltonian (or Lagrangian) of the system or directly in the Newton's equation of motion with the Lorentz force. Applying the technique to a certain class of spherically symmetric charge distribution with no magnetic field can readily give the rate of expansion at any stage of the Coulomb explosion. Applying it to a uniformly charged cylinder in a uniform magnetic field along the cylinder axis provides a differential equation that predicts (1) the transverse-to-magnetic-field radius of the charge distribution oscillates with a frequency that is lower than the electron cyclotron frequency because of the self-Coulomb field, (2) a classical free electron gas (spinless, non-relativistic and point-like electrons) in free space is diamagnetic due to its self-magnetic field, and (3) the self-conductivity tensor has oscillating diagonal elements. The results are verified by N-body simulations.

1. Introduction

We have recently reported experiments in which the dynamics of a photoemitted electron gas inside a uniform magnetic field has been observed and characterized by ultrafast electron microscopy (UEM) [1]. The electron gas undergoes radial oscillations in the transverse-to-magnetic-field direction, and it behaves like a diverging electromagnetic lens with a time-varying strength affecting the imaging system of the UEM. These observations have motivated us to develop a mean field theory that describes the Coulomb explosion in a uniform magnetic field.

The study of the collective behavior of high-density charged particles distributions under their own electric field has been a topic of research in several different disciplines. Studies like Coulomb explosion of highly charged clusters or nano-scale targets induced by an ultrafast laser pulse [2-9], Coulomb explosion role in the laser-induced ablation [10-11], Coulomb explosion during a chemical reaction [12], space charge imaging of molecules [13-15], emission of highly charged electron pulses from various types of emitters and their energy spread [16-19], propagation of continuous or bunched electron beams in electron diffraction and imaging systems [20-26], in streak tubes [27] and in microwave tubes [28-29], etc. have made this topic of a crucial importance. A full description of many of the observed phenomena in these studies need a solid understanding of the Coulomb explosion dynamics. The conservation of energy, for instance, has been used to find the distance of an ion separated from its original cluster by an intense laser pulse [2,3,6] or to describe the shock waves in a continuous charge distribution model [4]. The kinetic energy is found by calculating the potential energy at the initial and later times, from which the velocity

of the separated ions can be achieved. Also, Vlasov-Poisson equation has been used to find the dynamics of accelerated ions that were released from symmetric nanoscale targets by a Coulomb explosion triggered by a laser pulse [9]. Another analytical method was to average the single-particle equation of motion over a particle phase space distribution [21-23]. Here, we use the charge-current continuity equation for a spherically symmetric continuous charge distribution to obtain the corresponding current density which is generated by the self-electric field of the distribution. From the current density, the drift velocity is calculated, which can be used to find the system's Hamiltonian (or Lagrangian) or to write the Newton's equation of motion directly. In the absence of magnetic field, this results in a differential equation that governs the dynamics of the system and matches the previously reported dynamics. This technique can be used for a variety of charge distributions of spherical symmetry and can be generalized to an ellipsoidal distribution which is briefly discussed in the current work.

If the Coulomb explosion occurs inside a uniform magnetic field, this technique is very efficient in determining the dynamics of the system when it has cylindrical symmetry. Dynamics of neutral and non-neutral plasmas inside a magnetic field has been a topic of interest especially in the field of cyclotron resonance mass spectroscopy, which is commonly used for high-precision determination of ion masses. In those devices, the detected signal has a frequency that deviates from the bare cyclotron one for three reasons [30]: (1) the confining fields of the trap (2) the image charges induced on trap conductive walls and (3) the self-field shifts [31-33], which can even include polarization forces in polar molecules [34]. It has been shown that the frequency drift due to the self-field depends on the density, shape of the cloud and trap geometry [35]. The geometry of the trap can affect the plasma mode due to the induced image charges [36]. Noticeably, spectrum broadenings and shifts in the cyclotron resonance have also been observed inside materials that were attributed to the Coulomb interactions [37-42]. In our model, the Coulomb expansion in a magnetic field takes place in free space with no boundaries, i.e. there are no induced image charges and hence we only expect to observe the lowest mode of radial oscillation, namely the radial breathing mode [36]. We find a non-linear differential equation governing the radius of the charge distribution as a function of time, solve it numerically and compare the results to that of N-body simulations. The analytical model reveals a redshift and chirp in the radial oscillations frequency due to the Coulomb explosion, the diamagnetism of the electron gas and the oscillatory nature of the self-conductivity tensor elements.

In Section 2 of this paper, we describe the method of using the current density to determine the dynamics of a Coulomb explosion without a magnetic field and compare it to the results of N-body simulations as well as those previously published on this topic. In Section 3, we use the method to analyze the effect of the magnetic field on the expansion of the charge distribution. There are three functions and parameters that we compare between the two sections: (1) the asymptotic behaviors of the self-electric fields, (2) the temperatures of the clouds and (3) their self-conductivities which we define as a tensor relating the current density vector to the self-electric field vector. The magnetic field has a profound effect on all of them. It results in a self-magnetic field of the expanding electron cloud that opposes the external one, i.e. a classical electron gas is diamagnetic in agreement with the fact that a rotating plasma can be diamagnetic [43-46]. We prove this by not only finding the self-magnetic field from the theory and compare it to the result of an N-body simulation, but also by determining the magnetic moment of the cloud. The self-magnetic field results in a second-order self-electric field that will be discussed in Section 3 as well.

2. Expansion of spherical charge distribution under its self-Coulomb field with no magnetic field

We assume a spherically symmetric uniformly charged cloud of electrons evolving under its self-Coulomb force. The time-dependent charge density for N electrons can be written as

$$\rho(R, t) = \frac{-3Ne}{4\pi R_0^3(t)} U\left(1 - \frac{R}{R_0(t)}\right) = \frac{-3Ne}{4\pi (5\sigma_R^2(t))^{3/2}} U\left(1 - \frac{R}{\sqrt{5}\sigma_R(t)}\right), \quad (1)$$

where $R_0(t)$ is the time-varying radius of the electron cloud and $\sigma_R(t)$ its standard deviation (std) and $U(\cdot)$ is the Heaviside function

$$U(x) = \begin{cases} 0 & x < 0 \\ 1 & x \geq 0 \end{cases}. \quad (2)$$

By solving the continuity equation

$$\frac{\partial}{\partial t} \rho(R, t) = -\nabla \cdot \mathbf{J}, \quad (3)$$

the current density \mathbf{J} becomes

$$\mathbf{J}(R, t) = \frac{\sigma_R(t)}{\sigma_R(t)} R \rho(R, t) \hat{\mathbf{R}}, \quad (4)$$

beside a curl of an arbitrary function which is considered zero due to symmetry. The dot operator in Eq. (4) represents the time derivative. From the equation $\mathbf{J} = \mathbf{v}\rho$, the average drift velocity will be

$$\mathbf{v}(R, t) = \frac{\dot{\sigma}_R(t)}{\sigma_R(t)} R \hat{\mathbf{R}}. \quad (5)$$

Having $\mathbf{v}(R, t)$, the total kinetic energy of the cloud will be

$$KE = -\frac{1}{2} \frac{m}{e} \int \rho(R, t) \mathbf{v}^2(R, t) dV = \frac{3Nm}{2} \dot{\sigma}_R^2(t). \quad (6)$$

Comparing this result to the kinetic energy of a gas with three degrees of freedom per particle reveals that $\dot{\sigma}_R(t)$ is equal to the velocity spread. The total potential energy of the given charge distribution is

$$W = \frac{N^2 e^2}{4\pi\epsilon_0} \frac{3}{5R_0(t)} = \frac{N^2 e^2}{4\pi\epsilon_0} \frac{3}{5^{3/2} \sigma_R(t)}, \quad (7)$$

and the conservation of total energy, $W + KE = \text{constant}$, gives

$$\dot{\sigma}_R^2 + \frac{Ne^2}{2\pi 5^{3/2} m \epsilon_0} \frac{1}{\sigma_R} = \dot{\sigma}_{R0}^2 + \frac{Ne^2}{2\pi 5^{3/2} m \epsilon_0} \frac{1}{\sigma_{R0}}, \quad (8)$$

where

$$\sigma_{R0} = \sigma_R(0), \quad \dot{\sigma}_{R0} = \left. \frac{d\sigma_R}{dt} \right|_{t=0}. \quad (9)$$

Taking a derivative of both sides with respect to time will give

$$\ddot{\sigma}_R(t) = \frac{Ne^2}{4\pi 5^{3/2} m \epsilon_0} \frac{1}{\sigma_R^2(t)}. \quad (10)$$

Note that Eq. (10) is the Euler-Lagrange equation corresponding to the Lagrangian

$$\mathcal{L} = \frac{3Nm}{2} \dot{\sigma}_R^2(t) - \frac{N^2 e^2}{4\pi \epsilon_0} \frac{3}{5^{3/2} \sigma_R(t)}. \quad (11)$$

The other method to obtain the equation of motion is to use the Lorentz force. The non-relativistic equation of motion

$$m \frac{d}{dt} \mathbf{v} = -e \mathbf{E} \quad (12)$$

with the material derivative

$$\frac{d}{dt} \mathbf{v} = \frac{\partial}{\partial t} \mathbf{v} + \mathbf{v} \cdot \nabla \mathbf{v} \quad (13)$$

and the interior electric field of a uniformly charged sphere

$$\mathbf{E} = -\frac{NeR \hat{\mathbf{R}}}{4\pi \epsilon_0 (5\sigma_R^2(t))^{3/2}} \quad (14)$$

give

$$m \frac{d}{dt} \left(\frac{\dot{\sigma}_R(t)}{\sigma_R(t)} \right) R + m \left(\frac{\dot{\sigma}_R(t)}{\sigma_R(t)} \right)^2 R = \frac{Ne^2 R}{4\pi \epsilon_0 (5\sigma_R^2(t))^{3/2}}, \quad (15)$$

which after simplifications, leads to Eq. (10). In the literature, this type of equations is called envelope equation [22]. Eq. (8) have an exact implicit solution

$$t = \frac{A}{C^{3/2}} \ln \left(\frac{\sqrt{C^2 \sigma_R(t) - AC} + \sqrt{C^2 \sigma_R(t)}}{\sqrt{C^2 \sigma_{R0} - AC} + \sqrt{C^2 \sigma_{R0}}} \right) + \frac{1}{C} \left(\sqrt{C \sigma_R^2(t) - A \sigma_R(t)} - \sqrt{C \sigma_{R0}^2 - A \sigma_{R0}} \right), \quad (16)$$

for

$$A = \frac{Ne^2}{2\pi 5^{3/2} m \epsilon_0}, C = \dot{\sigma}_{R0}^2 + \frac{A}{\sigma_{R0}}. \quad (17)$$

If the cloud has no initial velocity spread, then C will have its lowest value $C = A/\sigma_{R0}$ and Eq. (16) becomes

$$t = \frac{\sigma_{R0}}{\sqrt{C}} \left\{ \ln \left(\sqrt{\frac{\sigma_R(t)}{\sigma_{R0}}} - 1 + \sqrt{\frac{\sigma_R(t)}{\sigma_{R0}}} \right) + \sqrt{\left(\frac{\sigma_R(t)}{\sigma_{R0}} \right)^2 - \frac{\sigma_R(t)}{\sigma_{R0}}} \right\}, \quad (18)$$

which is similar to what is reported in [5]. Note that in these calculations, the assumption is that only the mean field is responsible in converting the potential energy to kinetic energy; for example, no stochastic processes are included.

Fig. 1 (a) compares the time-varying spatial std of a uniformly charged sphere filled with 10,000 electrons with no initial velocity obtained from Eq. (18) to that from an N-body simulation. The comparison is done for two initial stds of 2 μm and 5 μm . The details of the simulation are given in Appendix A.

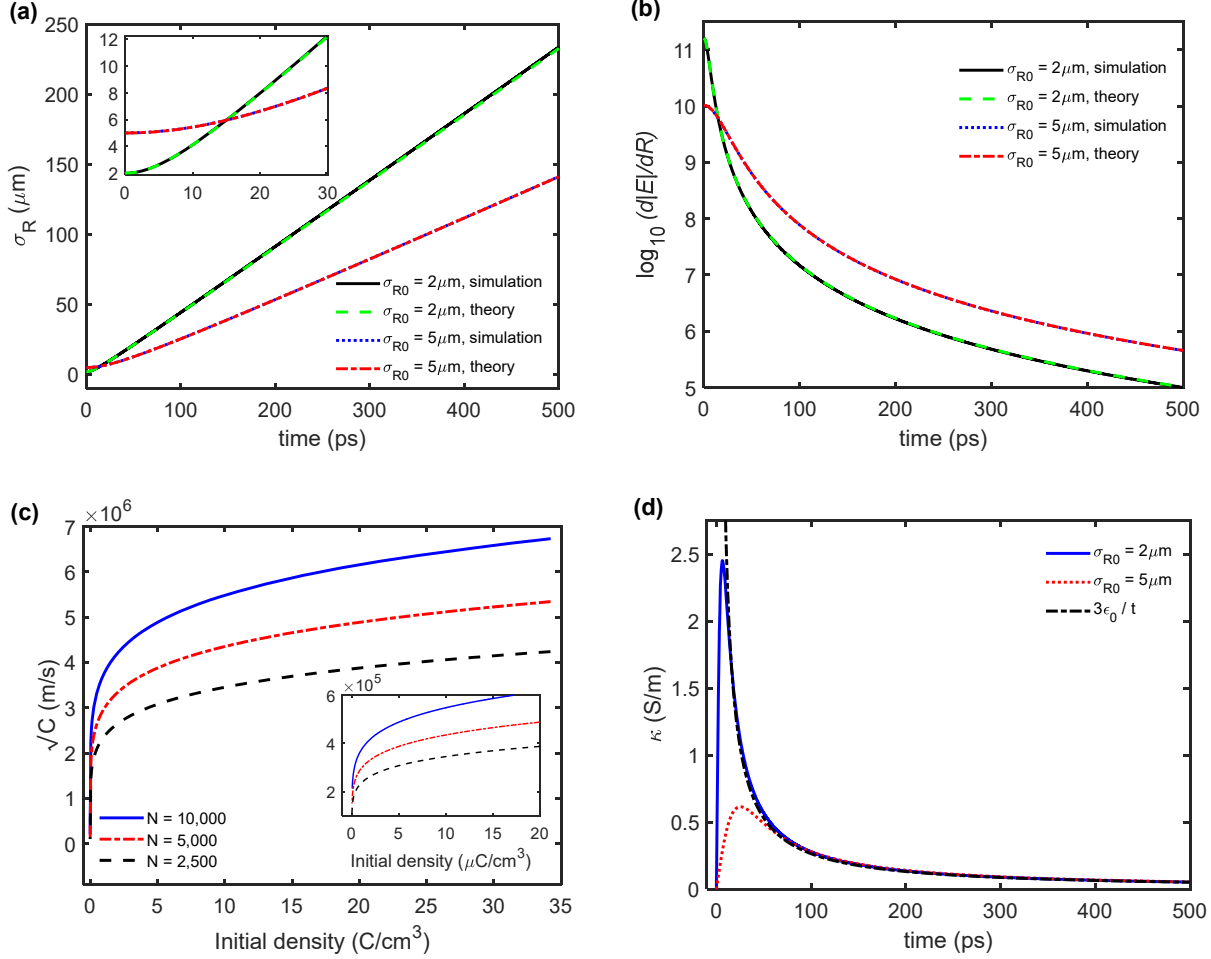


Fig. 1 Comparison of the simulated and the theoretical Coulomb explosion dynamics of a uniformly charged sphere containing 10,000 electrons with no initial velocity for two initial dimensions of 2 μm and 5 μm (std) (a) Spatial stds as functions of time obtained from N-body simulation and the analytical solution in Eq. (18) (b) $d|E|/dR$ on a logarithmic scale as a function of time, calculated from the N-body simulation and also by Eq. (14). A higher initial charge density leads to a lower electric field at later times due to a faster expansion. (c) The final rate of expansion of the spatial std of the distribution as a function of initial charge density for three numbers of electrons. The final expansion velocities for low initial densities is depicted in the inset. (d) The self-conductivities of two freely expanding electron gases as functions of time. Regardless of the initial charge density, the self-conductivity always converges to $3\epsilon_0/t$ which is included in the figure as well.

Inserting Eq. (20) into Eq. (14), the electric field will be

$$\mathbf{E} \approx -\frac{NeR\hat{\mathbf{R}}}{4\pi\epsilon_0(5Ct^2)^{3/2}} = -\sqrt{\frac{\epsilon_0\pi}{2N}} \frac{(m5^{1/2}\sigma_{R0})^{3/2}R\hat{\mathbf{R}}}{e^2t^3}. \quad (19)$$

Therefore, the asymptotic electric field will be inversely proportional to the square root of the initial charge density which is counterintuitive as it cannot be seen directly from the Maxwell-Gauss equation. In Fig. 1 (b), the logarithm of $d|E|/dR$ versus time is plotted for both the N-body simulation and the analytical solution. The charge distribution with ~ 16 times higher initial charge density produces smaller electric field ~ 15 ps after the explosion starts at the same distance from the charge distribution center of mass.

When $\sigma_R(t) \gg \sigma_{R0}$ for $t \rightarrow \infty$, Eq. (18) can be approximated by

$$\sigma_R(t) \approx \sqrt{C}t. \quad (20)$$

Quantity \sqrt{C} has the unit of velocity and is the asymptotic rate of expansion, which depends on $\sqrt{N/\sigma_{R0}}$. For example, the spatial std of a uniformly charged sphere with a radius of $2\sqrt{5} \mu\text{m}$ containing 10,000 electrons at rest will reach the final expansion rate of $4.765 \times 10^5 \text{ m/s}$ obtained from the simulation while for the same charge distribution $\sqrt{C} = 4.759 \times 10^5 \text{ m/s}$. The value of \sqrt{C} as a function of the initial density for three different numbers of electrons initially at rest is plotted in Fig. 1 (c).

The self-conductivity κ can be defined by $\mathbf{J} = \kappa\mathbf{E}$. By using the current density and the electric field in Eq. (4) and (14), respectively, we will have

$$\kappa = 3\epsilon_0 \frac{\sigma_R(t)}{\sigma_R(t) \xrightarrow{t \rightarrow \infty} \frac{3\epsilon_0}{t}}, \quad (21)$$

which is a scalar quantity. In the next section, we will show how an external magnetic field will change κ to a tensor whose diagonal elements oscillate by time. Fig. 1 (d) shows the self-conductivity for two different initial charge distributions as a function of time calculated by the simulation. There also is plotted the asymptotic value of the self-conductivity in Eq. (21) which is independent of the initial charge density.

The final temperature of a freely expanding charge distribution with no initial velocity is

$$T(t \rightarrow \infty) = \frac{3m}{2k} \sigma_R^{-2}(t \rightarrow \infty) \rightarrow \frac{3m}{2k} C = \frac{3Ne^2}{4\pi 5^{3/2} k \epsilon_0 \sigma_{R0}} \approx 4.5 \times 10^{-6} \frac{N}{\sigma_{R0}}, \quad (22)$$

and is equal to the maximum potential energy (at time zero) divided by kN where k is the Boltzman constant. For example, an electron gas consisting of 10,000 electrons with an initial std deviation of $5 \mu\text{m}$ and zero initial temperature, will reach the final temperature of 9,000 K.

The technique of using the current density can be generalized to some other distributions. Suppose we have a spherically symmetric charge distribution of the following form

$$\rho(R, t) = \frac{3Ne}{4\pi\sigma_R^3(t)} f(R, \sigma_R(t)), \quad (23)$$

where $f(\cdot)$ is a unitless function whose volume integral over the whole space is unity. If we demand that the corresponding current density be of the form in Eq. (4), then for the continuity equation to hold we must have

$$f(R, \sigma_R(t)) = f\left(\frac{R}{\sigma_R(t)}\right). \quad (24)$$

The proof is given in Appendix B. Examples of this class of distributions are uniform distribution, Gaussian distribution, raised cosine distribution, triangle distribution, Wigner semicircle distribution, and any other distribution whose std scales linearly with coordinate. However, the non-relativistic uniform distribution is the only one that maintains its profile as it evolves in time. It is because in Eq. (15), every term is linear in R and hence the final equation of motion is independent of it. Therefore, this technique is expected to provide only an approximate solution for the other distributions that satisfy Eq. (24).

As an example, for a Gaussian charge distribution

$$\rho(R, t) = -Ne \frac{e^{-R^2/2\sigma_R^2(t)}}{(2\pi)^{3/2}\sigma_R^3(t)}, \quad (25)$$

we can find the non-relativistic kinetic energy $KE = \frac{3Nm}{2}\sigma_R^2(t)$, and the total potential energy

$$W = \frac{\epsilon_0}{2} \int dV |\mathbf{E}|^2 = \frac{\sqrt{\pi}}{2} \frac{N^2 e^2}{(2\pi)^2 \epsilon_0} \frac{1}{\sigma_R(t)}. \quad (26)$$

And use the conservation of energy to find

$$\sigma_R^2(t) + \frac{Ne^2}{12\pi^2 m \epsilon_0} \frac{1}{\sigma_R(t)} = \text{constant}. \quad (27)$$

But this assumes that a Gaussian charge distribution maintains its Gaussian profile as it evolves which is not a valid assumption [26]. Nevertheless, we use this theory to evaluate $\sigma_R(t)$ and for $R < \sigma_R(t)$, the Gaussian distribution can be approximated by a uniform distribution according to its Taylor series expansion. Therefore, we expect this equation, though approximate, to be of good accuracy. Eq. (27) has the similar solution given in Eq. (16) but for

$$A = \frac{Ne^2}{12\pi^2 m \epsilon_0} \quad (28)$$

Fig. 2 depicts the accuracy of this method for a Gaussian charge distribution by comparing its spatial std obtained from an N-body simulation with that of the analytical method presented here for 10,000 electrons with no initial velocity and 5 μm initial spatial std. Comparing Eq. (27) to Eq. (8), the Gaussian charge distribution has a slightly faster rate of expansion (it is about 1.0253 times faster).

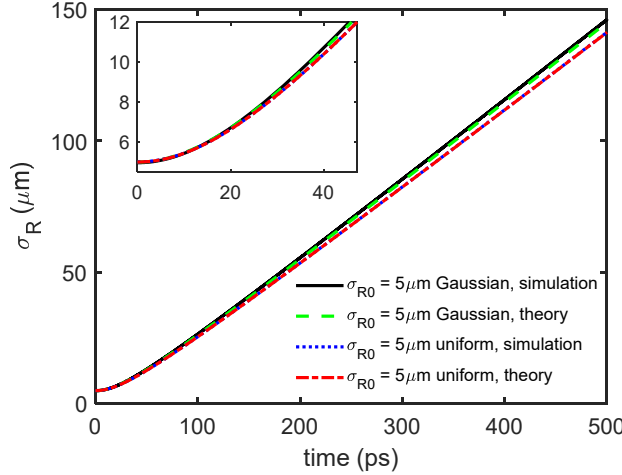


Fig. 2 Expansion of a spherical Gaussian charge distribution consisting of 10,000 electrons under its self-electric field with no initial velocity calculated both from the N-body simulation and the theory. Dynamics of a uniformly charged sphere is included for comparison.

For the general case of a non-relativistic expansion of a spherical charge distribution with an arbitrary initial density, we have given a nonlinear integrodifferential equation in Appendix C that governs the full dynamics of the charge distribution. Solving such an equation is beyond the scope of this work.

For the case that the uniform distribution is not spherically symmetric, but for example ellipsoidal, one can generalize the method by finding the corresponding asymmetrical drift velocity vector, the kinetic energy and the potential energy of the distribution and form the Lagrangian of the system. This leads to three coupled differential equations that govern the dynamics of the system.

In the next section, we will use the same technique explained here to model the behavior of a charge distribution expanding under its own electric field and an external magnetic field.

3. Coulomb explosion inside a uniform magnetic field

A spherical charge distribution placed in a uniform magnetic field will not maintain its sphericity because the magnetic field bends the trajectory of the electrons in the plane transverse to it and confines the charges as much as the self-electric field of the distribution allows. The charge distribution, however, will expand freely in the axial direction. So, the charge distribution will become prolate. Here, for the sake of simplicity, we consider a uniformly charged cylinder with a circular cross section inside a uniform magnetic field along its axis as a generic analytical model. The charge density is

$$\rho = -\frac{n_z e}{\pi r_0^2(t)} U\left(1 - \frac{r}{r_0(t)}\right) \quad (29)$$

in the cylindrical coordinate (r, ϕ, z) , where the Heaviside function $U(\cdot)$ is given by Eq. (2), and n_z is the number of electrons per unit length in the z direction, i.e. the projection of ρ on the z axis, which will be a constant for an infinitely long charge distribution in z because of symmetry. For this distribution, a current density that satisfies the continuity equation is

$$\mathbf{J} = -\frac{n_z e}{\pi r_0^2(t)} \left(\frac{\dot{r}_0(t)}{r_0(t)} r \hat{\mathbf{r}} + g(r) \hat{\boldsymbol{\phi}} \right) U \left(1 - \frac{r}{r_0(t)} \right), \quad (30)$$

where the $\hat{\boldsymbol{\phi}}$ component is divergence-free and accounts for the effect of the external uniform magnetic field in the $+z$ direction that leads to $\mathbf{E} \times \mathbf{B}$ drift. The function $g(r)$ will be determined by the dynamics of the system. The electric field of this distribution is obtained from the Maxwell-Gauss equation $\nabla \cdot \mathbf{E} = \rho/\epsilon_0$ as

$$\mathbf{E} = -\frac{n_z e r}{2\pi\epsilon_0 r_0^2(t)} \hat{\mathbf{r}}. \quad (31)$$

The non-relativistic equation of motion, when the self-field momentum is negligible, is

$$m \left(\frac{\partial \mathbf{v}}{\partial t} + \mathbf{v} \cdot \nabla \mathbf{v} \right) = \frac{n_z e^2 r}{2\pi\epsilon_0 r_0^2(t)} \hat{\mathbf{r}} - e \mathbf{v} \times B_0 \hat{\mathbf{z}}, \quad (32)$$

where $B_0 \hat{\mathbf{z}}$ is the external magnetic field, and the drift velocity \mathbf{v} is obtained by Eq. (30) as

$$\mathbf{v} = \frac{\mathbf{J}}{\rho} = \frac{\dot{r}_0(t)}{r_0(t)} r \hat{\mathbf{r}} + g(r) \hat{\boldsymbol{\phi}}. \quad (33)$$

The azimuthal component of the equation of motion gives

$$r \frac{dg(r)}{dr} + g(r) = \frac{eB_0}{m} r, \quad (34)$$

with an acceptable solution of

$$g(r) = \frac{eB_0}{2m} r. \quad (35)$$

The quantity $eB_0/2m$ is the angular frequency of a classical rotating body with a gyromagnetic ratio of $\gamma = Ne/2Nm$ where Ne and Nm are its total charge and mass, respectively. This frequency is half of the cyclotron angular frequency eB_0/m . Note that the self-Coulomb field does not affect the azimuthal component of the current density which is expected because the Coulomb force is an internal force. This result also can be verified by calculating the mechanical angular momentum per unit length of the charge distribution

$$\frac{d\mathbf{L}_m}{dz} = -\frac{m}{e} \int_{r=0}^{r_0(t)} \int_{\phi=0}^{2\pi} \mathbf{r} \times \mathbf{J} r dr d\phi = \frac{n_z e B_0}{4} r_0^2(t) \hat{\mathbf{z}}, \quad (36)$$

and the zz component of the moment of inertia tensor per unit length

$$\frac{dI_{zz}}{dz} = \frac{n_z m}{2} r_0^2(t). \quad (37)$$

Comparing these two equations gives the same angular frequency of $eB_0/2m$. Note that the mechanical angular momentum is not a conserved quantity but the total angular momentum, including the field momentum, is. The field momentum per unit length $d\mathbf{L}_f/dz$ is

$$\frac{d\mathbf{L}_f}{dz} = \int_{r=0}^{r_0(t)} \int_{\phi=0}^{2\pi} \mathbf{r} \times \mathbf{A}_0 \rho \, r dr d\phi = \int_{r=0}^{r_0(t)} \int_{\phi=0}^{2\pi} \mathbf{r} \times \frac{B_0 r}{2} \hat{\phi} \rho \, r dr d\phi = -\frac{n_z e B_0}{4} r_0^2(t) \hat{\mathbf{z}}, \quad (38)$$

where $\mathbf{A}_0 = \frac{B_0 r}{2} \hat{\phi}$ is the magnetic vector potential associated with the external magnetic field. From Eq. (36) and (38), it is seen that the total angular momentum of the system, as expected, is zero. Note that we treated the charge distribution as a classical rotating body whose angular frequency of rotation depends on the magnetic field. The important conclusion is that the frequency of the rotation does not change as the radius of the charge density varies by time since the mechanical angular momentum is not conserved.

By use of Eq. (35), the radial component of equation of motion in Eq. (32) becomes

$$r_0''(t) + \left(\frac{eB_0}{2m}\right)^2 r_0(t) = \frac{n_z e^2}{2\pi m \epsilon_0 r_0(t)}. \quad (39)$$

In this model, the force due to the magnetic field is effectively, but not truly, in the radial direction and is a restoring force responsible for diminishing the radius of the charge distribution.

Parallel to the previous section, Eq. (39) can be obtained from the conservation of energy, provided the energy leaving the system by radiation is negligible. The kinetic energy per unit length in z can be calculated from the drift velocity in Eq. (33) and the mass distribution as

$$\frac{d}{dz} KE = -\pi \frac{m}{e} \int \rho v^2 r dr = \frac{n_z m}{4} \left(\dot{r}_0^2 + \left(\frac{eB_0}{2m}\right)^2 r_0^2 \right). \quad (40)$$

The zero of the potential energy can be assumed at the largest radius of the charge distribution r_M which is a return point and hence $\dot{r}_M = 0$. Therefore, the total energy of the system per unit length in z is

$$\frac{d}{dz} U = \frac{n_z m}{4} \left(\frac{eB_0}{2m}\right)^2 r_M^2 \quad (41)$$

At first glance, it is surprising that the total energy depends on the magnetic field because the magnetic field does not work. The magnetic field only affects the way the electric field works, i.e. the rate at which the kinetic and potential energies are converted to each other. As a result, r_M must inversely depend on B_0 , such that the *total* derivative of the internal energy with respect to the magnetic field always vanishes.

Setting the zero of the potential energy at $r_0(t) = r_M$ will determine the potential energy per unit length in z as

$$\frac{d}{dz} W = \frac{n_z^2 e^2}{4\pi \epsilon_0} \left(\ln \frac{r_M}{r_0(t)} \right), \quad (42)$$

where $\ln(\cdot)$ is the natural logarithm function. Then, the conservation of energy dictates

$$\frac{d}{dz} U = \frac{n_z m}{4} \left(\dot{r}_0^2 + \left(\frac{eB_0}{2m}\right)^2 r_0^2 \right) + \frac{\epsilon_0 n_z^2 e^2}{4\pi \epsilon_0} \left(\ln \frac{r_M}{r_0(t)} \right) = \frac{n_z m}{4} \left(\frac{eB_0}{2m}\right)^2 r_M^2. \quad (43)$$

If we take the time-derivative of both sides of the above equation and simplify it, we will get Eq. (39). One can find the same results by use of the Lagrangian of the system as well.

To the best knowledge of the authors, Eq. (39) does not have an analytical closed-form solution. Without the self-Coulomb field on the right-hand-side, the solution to this equation will be

$$r_0(t) = r_M \sqrt{\frac{1}{2} - \frac{1}{2} \cos \left(\frac{eB_0}{m} t + \varphi \right)}, \quad (44)$$

where the charge distribution oscillates radially between zero and r_M with an initial arbitrary phase φ and the cyclotron angular frequency of eB_0/m . The self-Coulomb field will prevent the charge distribution from reaching the zero radius, i.e. from a full collapse on the z axis.

If, at the time zero, the external magnetic field satisfies

$$B_0 = \sqrt{\frac{2mn_z}{\epsilon_0 \pi r_0^2(0)}} = \sqrt{2} \frac{m}{e} \omega_{pe0} \quad (45)$$

where ω_{pe0} the plasma frequency at the initial time, and the electrons have no initial velocity, there will be no oscillation since the driving forces due to the self-electric field and the external magnetic field in Eq. (39) cancel out and the charge distribution will maintain its initial radius. However, in compliance to the Earnshaw's theorem, it is an unstable equilibrium because any small change in any of the system parameters will lead to an oscillation.

Eq. (39) suggests that the self-Coulomb force can change the frequency of oscillation in a nontrivial way. The frequency of radial expansion and contraction of the charge distribution for $B_0 = 0.25$ T, $r_0(t = 0) = \sqrt{5} \mu\text{m}$ a range of $n_z = 100$ to 10^{12} electrons per meter with no initial velocity is numerically obtained and sketched in Fig. 3. Note that Eq. (39) is stiff, i.e. to solve it numerically by the finite difference method, an extremely small temporal step size of 2 attosecond was need for convergence of the solution. At low values of n_z , the electron distribution will be more granular rather than continuous and the analytical method, developed here, will not be accurate. As we will show later, beyond $n_z = 10^{12}$ electrons per meter, the self-magnetic field and second-order self-electric field will emerge. There is an antiresonance, as explained above, happening at $n_z \approx 4.77 \times 10^6$ electrons per meter for which Eq. (45) is satisfied.

Here, we would like to distinguish between the cyclotron frequency and the frequency of radial expansion and contraction. The former is fixed and twice the rotational frequency of the charge distribution which is unaffected by the Coulomb interaction. We do this to abide by the Kohn's theorem that shows, at the quantum level, the cyclotron oscillation frequency is independent of the Coulomb interactions [47].

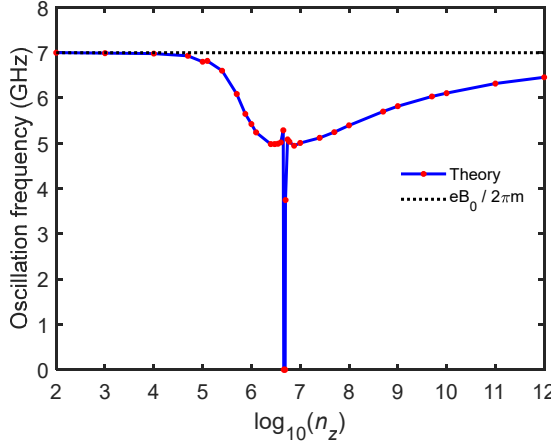


Fig. 3 The oscillation frequency of radial contraction and expansion of a uniformly charged cylinder under a uniform magnetic field of 0.25 T along its axis for various charge density (number of electrons per unit length along the cylinder axis) with an initial diameter of 4.47 μm and no initial velocity. The space charge reduces the oscillation frequency from the nominal value of $eB_0/2\pi m = 6.998 \text{ GHz}$ which is included for comparison. The frequency is obtained by numerically solving Eq. (39). The antiresonance happening at $n_z \approx 4.77 \times 10^6$ electrons per meter is because the electric and magnetic forces cancel out and the charge distribution will not oscillate. It represents an unstable equilibrium.

No charge distribution will be infinitely long; subsequently n_z will not be a constant but a function of time. If $n_z(t)$ is a slow function of time in comparison to $r_0(t)$, Eq. (39) can be employed to determine the dynamics of the system. Indeed one can show that if n_z decreases linearly by time, Eq. (39) will remain unchanged; however, the nature of the solution and frequency shifts can be very different since it is a nonlinear differential equation. The results of an N-body simulation together with a numerical evaluation of Eq. (39) is shown in Fig. 4 (a). In the simulation, at time zero, 10,000 at rest electrons are distributed uniformly by a random process inside a prolate spheroid with the small and long diameters of $2r_0(t=0) = 2\sqrt{5} \mu\text{m}$ and $2h_0(t=0) = 20\sqrt{5} \mu\text{m}$ respectively, inside a uniform magnetic field of 0.25 T along the longer axis of the distribution (details are given in Appendix A). The simulation time step is 80 fs. According to the simulation results, the distribution expands almost freely in the z direction and shows the radial oscillations. The electrons distribution at three points in time is illustrated in Fig. 4 (b). (The full movie of the electrons in the external magnetic field can be found in the Supplement Material 1). For such a distribution, it is straightforward to show that

$$n_z(t, z) = \frac{N}{\frac{4}{3}h_0(t)} \left(1 - \left(\frac{z}{h_0(t)} \right)^2 \right), \quad (46)$$

which we approximate by

$$n_z(t) \approx \frac{N}{\Delta z_{FWHM}} = \frac{N}{\sqrt{2}h_0(t)} = \frac{N}{\sqrt{10}\sigma_z(t)}, \quad (47)$$

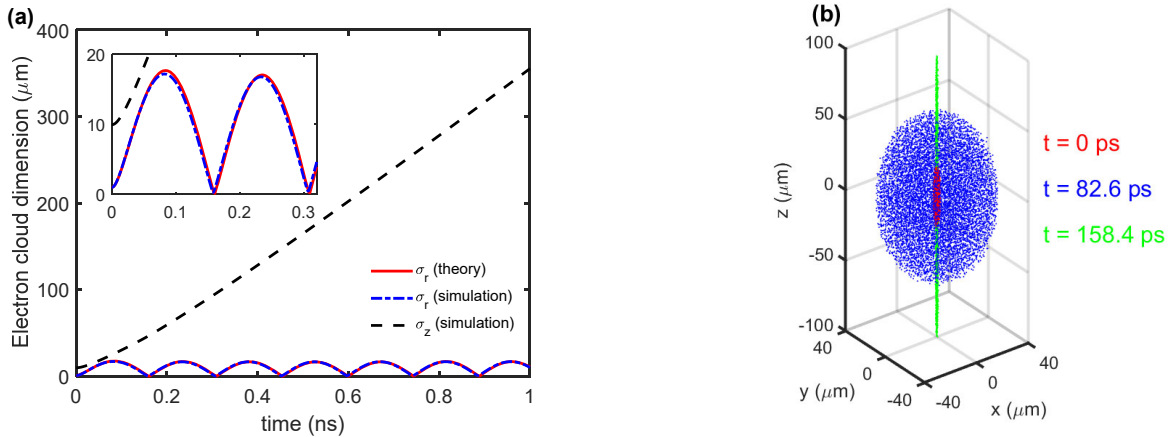
where Δz_{FWHM} is the full width half maximum of $n_z(t, z)$ in Eq. (46), which is plotted in Fig. 4 (c) as a function of time, together with the aspect ratio of the charge distribution. In the analytical model, we call $\sigma_z(t)$ from the simulation, calculate $n_z(t)$ from Eq. (47) and insert it into Eq. (39) and solve it numerically. The radial oscillation frequency from the simulation is obtained from the average distance between its

minima in the time interval of zero to 1 ns and is equal to 6.874 GHz. Doing the same for the theoretical results gives 6.873 GHz. The oscillation frequency given by the cyclotron equation is $eB_0/2\pi m = 6.998$ GHz. The reduction in the frequency is considerably less than what is predicted in Fig. 3 for a fixed value of n_z . Table 1 depicts the locations of the minima in the theory and simulation. There is a small chirp in the frequency seen in both methods. It means the distance between the minima gradually decreases by time in a nonlinear but monotonic fashion. The small differences between the theory and the simulation are most likely due the approximations in the theoretical model including the neglect of stochastic processes. The average and std of the electron cloud kinetic energy, obtained from the simulation, is shown in Fig. 4 (d). Local minima happen at times the charge distribution collapses along the z-axis. The radial component of the mean-field electric field of the cloud is calculated from the simulation and Eq. (31) and its derivative with respect to r is plotted in Fig. 4 (e) in a logarithmic scale. In the simulation, the mean field is obtained by a linear regression between the forces on the particles and their position vectors. The maxima of the electric field are higher in the theory due to the fact that the theory gives a slightly lower radius of the charge distribution at its minima. It is most likely because the theory is based on the mean field and does not capture the effect of collisions.

The self-conductivity tensor $\bar{\kappa}$ can be calculated by Eq. (30) and (31) in Cartesian coordinates

$$\bar{\kappa} = 2\epsilon_0 \begin{bmatrix} \frac{r_0(t)}{r_0(t)} & -\frac{eB_0}{2m} \\ \frac{eB_0}{2m} & \frac{r_0(t)}{r_0(t)} \end{bmatrix}, \quad (48)$$

which shows oscillating diagonal elements. The self-conductivity here is different from the one in Eq. (21) just because of the applied magnetic field. The components of the self-conductivity tensor, calculated from the theory and the simulation, are plotted in Fig. 4 (f).



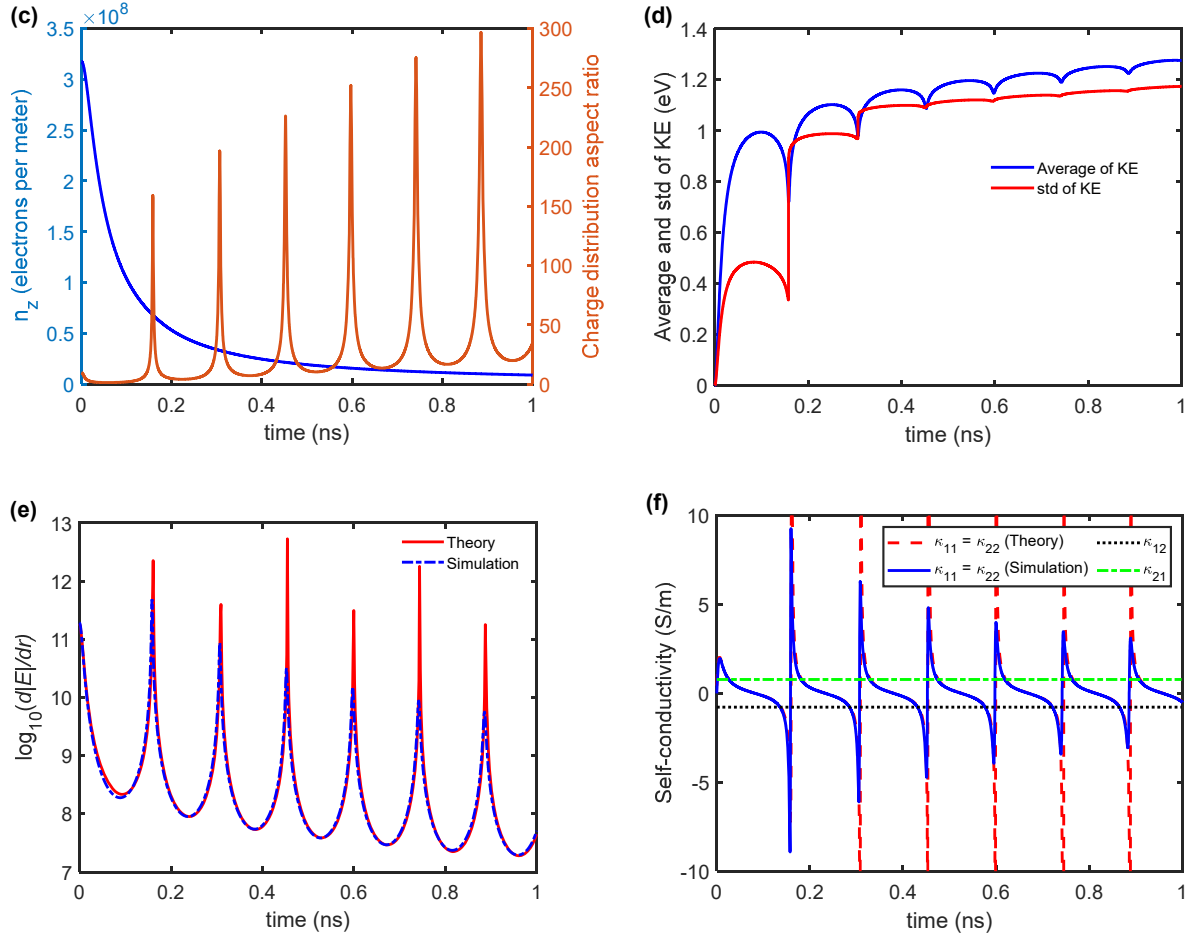


Fig. 4 (a) Dynamics of a uniform oblate spheroid charge distribution with initial transverse and axial diameters of $4.47 \mu\text{m}$ and $44.7 \mu\text{m}$, respectively and no initial velocity under a uniform magnetic field of 0.25 T along its long axis determined by an N-body simulation together with the analytical solution in Eq. (39). The two solutions match each other well. The inset shows the dynamics in the early stages of evolution. Minor differences are due to the approximations made in the theory. (b) The charge distribution from N-body simulation at three points in time: time zero, its first radial maximum and the minimum after. (c) n_z and the aspect ratio of the charge distribution as functions of time. n_z is obtained from the simulation and fed into the analytical model. (d) The average and std of the cloud kinetic energy vs time determined by the simulation. There are local minima happening at the minima of transverse radius of the electron cloud. (e) $d|E|/dR$ in logarithmic scale as a function of time calculated from an N-body simulation and also by Eq. (30). (f) Components of the self-conductivity vs time calculated by the simulation and the theory. The difference between the theory and the simulation in the last two plots are due to the fact that the minimum radius of the charge distribution is slightly smaller in theory than in the simulation.

Table (1) Locations of the minima in the transverse radius of charge distribution calculated by N-body simulations and the analytical model.

Minima locations (ps)		Difference		Minima locations (ps)		Difference	
Simulation	Simulation	Theory	Theory	Theory	Theory	Theory	Theory
158.4	-	160.4	-				
306.6	148.2	308.7	148.3				
452.5	145.9	454.5	145.8				
597.4	144.9	599.5	145.0				
741.8	144.4	743.9	144.4				
885.8	144.0	888.0	144.1				

The current density in Eq. (30) with $g(r)$ in Eq. (35) will lead to a self-magnetic field. If we insert the current density and the electric field in Eq. (31) into the Maxwell's equation

$$\nabla \times \mathbf{B} = \mu_0 \mathbf{J} + \mu_0 \epsilon_0 \frac{\partial \mathbf{E}}{\partial t}, \quad (49)$$

we arrive at the self-magnetic field

$$\mathbf{B}_s = -\frac{n_z e^2 \mu_0 B_0}{4\pi m} \left(1 - \frac{r^2}{r_0^2(t)}\right) U \left(1 - \frac{r}{r_0(t)}\right) \hat{z}, \quad (50)$$

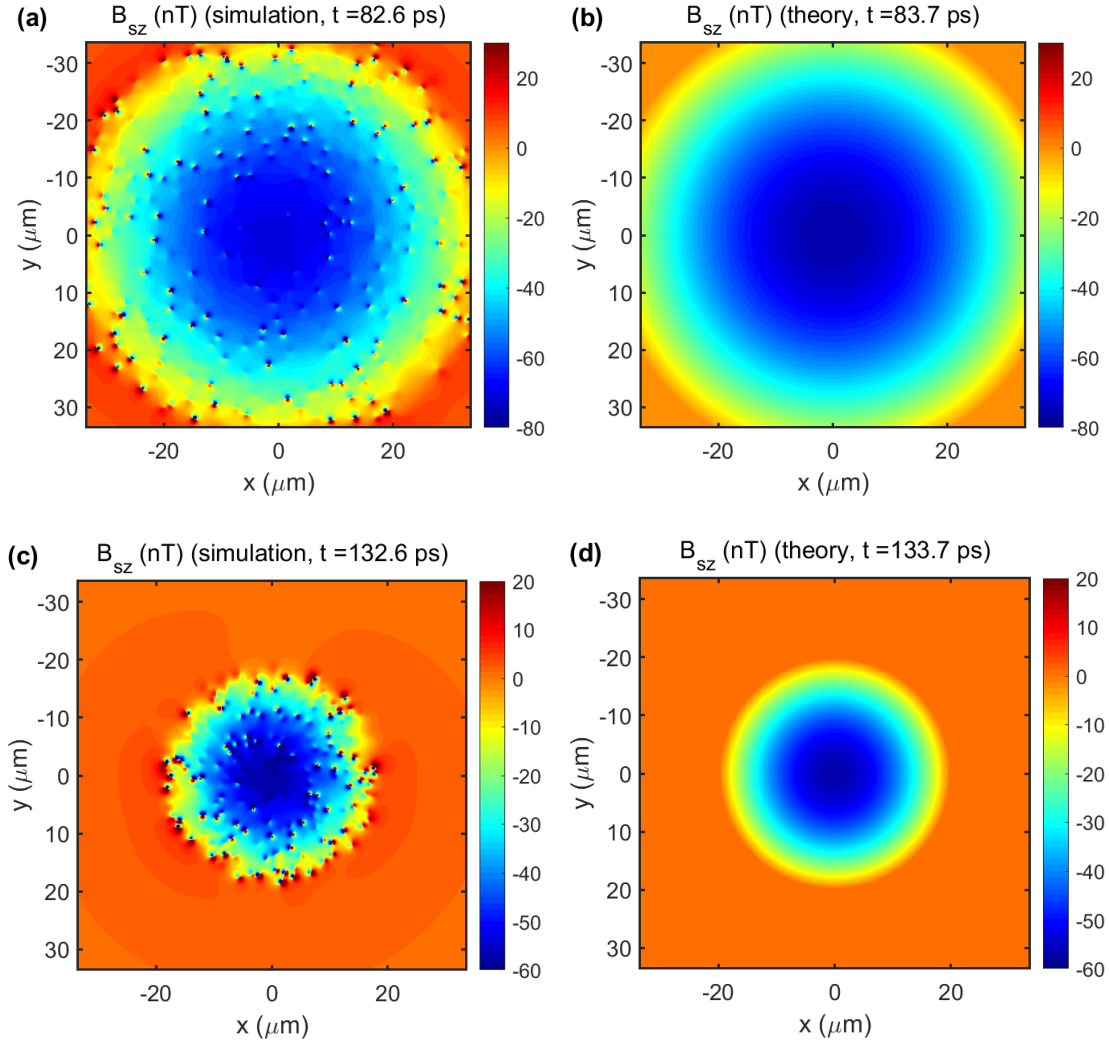
which opposes the external magnetic field, linearly depends on B_0 and shows that a free electron gas in free space is diamagnetic. This is not in contrast to the Bohr–van Leeuwen theorem because the whole system is macroscopically in rotation all the time according to the current density in Eq. (30). For the self-magnetic field be comparable to the external magnetic field, n_z must be of the order of $4\pi m/\mu_0 e^2 = 3.5 \times 10^{14}$ electrons per meter. The fact that the magnetic field is zero outside of the charge distribution is due to the infinite length of the charge distribution. For finite size charges, there will a magnetic field of opposite sign outside of the charge distribution because the magnetic field is divergence-free. The self-magnetic field, as expected is too small to affect the dynamics of the system. The self-magnetic field is plotted in Fig. 5 (a-d) at $z = 0$ calculated from the N-body simulation, as explained in Appendix A, and from Eq. (50) for n_z from Eq. (47) at two points in time: (1) at the first maximum radius of the charge distribution (2) at the midway between the first maximum and the second minimum. In Fig. 5 (e), their corresponding azimuthal average is plotted. At the first maximum, the charge distribution aspect ratio is only 1.5, so the theory deviates from the simulation. In the simulation, the magnetic field is positive outside of the charge distribution due to its finite longitudinal size. The local short-lived magnetic dipoles in the simulation are formed because of electron-electron short distance interactions, which are not included in the analytical model. Those interactions are more pronounced when the charge distribution reaches its radial minimum. The full video of the self-magnetic field is in Supplement Material 2.

The magnetic moment per unit length in z can be calculated by

$$\frac{d\mathbf{M}}{dz} = \frac{1}{2} \int_{r=0}^{r_0(t)} \int_{\phi=0}^{2\pi} \mathbf{r} \times \mathbf{J} r dr d\phi = -\frac{n_z e^2 B_0}{8m} r_0^2(t) \hat{\mathbf{z}}, \quad (51)$$

which suggests that a classical electron gas in a uniform magnetic field is diamagnetic. The *partial* derivative of Eq. (43) with respect to the negative of the magnetic field gives the magnetic moment per unit length in Eq. (51).

Note that according to kinetic energy in Eq. (40) the system is not at equilibrium and hence we cannot define an asymptotic temperature like in Eq. (22).



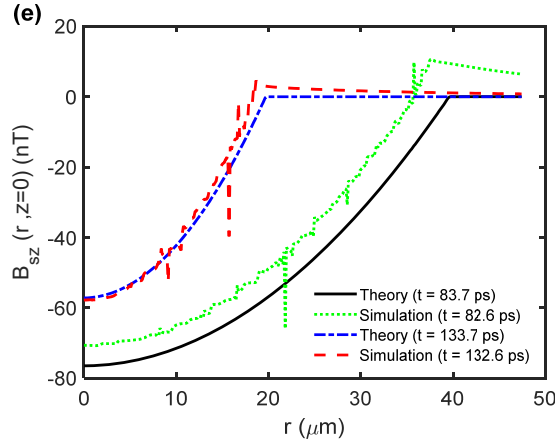


Fig. 5 Self-magnetic field at the first maximum of the charge distribution transvers radius by (a) the N-body simulation and (b) the theory. At that time, the charge distribution aspect ratio is only ~ 1.5 . The self-magnetic field is also plotted at the midpoint between the first maximum and the next minimum where the aspect ratio has increased to ~ 4.7 by (c) the N-body simulation and (d) the theory. The local magnetic dipoles in the simulation are due to electron-electron interactions and the resulting motion in the x-y plane. For all four cases, the azimuthal averages are plotted in part (e). When the aspect ratio is small the theory expectedly deviates from the simulation. The positive magnetic field outside of the charge distribution in the simulation is due to the limited size of the charge distribution in z and hence is absent in the theoretical model.

Having the self-magnetic field in Eq. (50), one can use the Maxwell-Faraday equation

$$\nabla \times \mathbf{E} = -\frac{\partial \mathbf{B}}{\partial t} \quad (52)$$

to find the second order self-electric field as

$$\mathbf{E}_s = -\frac{n_z e^2 \mu_0 B_0}{8\pi m} \dot{r}_0(t) \frac{r_0(t)}{r} \left(1 - \frac{r^4}{r_0^4(t)}\right) U \left(1 - \frac{r}{r_0(t)}\right) \hat{\phi} \quad (53)$$

(The first order self-electric field is given in Eq. (31)). Note that the sign of \mathbf{E}_s is opposite to that of $\dot{r}_0(t)$. That is due to the Lenz's law: as the charge distribution expands, the magnetic flux going through it increases, the induced electric field must generate a current whose magnetic field opposes the increase in the flux. The self-electric field in Eq. (53) is a result of the external magnetic field.

The technique we developed here to analyze a uniform cylindrical charge distribution under a uniform magnetic field can be generalized to other charge distributions like the Gaussian one.

4. Conclusion

In this work, we developed a technique that can determine the dynamics of electron distributions of high symmetry under their own electric field and an external magnetic field. We showed that the self-Coulomb field reduces the oscillation frequency of the charge density by numerically solving the differential equation that governs the system. The theory supports the idea that a classical electron gas in a uniform magnetic field is diamagnetic. The technique of using the current density to determine the dynamics of the charge distribution could also be used in less symmetric charge distributions, which will be the topic of future research. The far field radiation of such charge density is also of importance for instance in the field of cyclotron microwave spectroscopy as well as the radiation of pulsars in astrophysics.

Acknowledgement

We would like to thank Professor Phillip M. Duxbury and Dr. Brandon Zerbe from Michigan State University and Dr. Bryan W. Reed from Integrated Dynamic Electron Solutions, Inc. (IDES) for their very instructive discussions and comments on the theory.

This research was supported by a Packard Fellowship in Science and Engineering from the David and Lucile Packard Foundation

Appendix A: N-body simulation

The N-body simulation calculates the Lorentz force on each electron inside an electron cloud due to other charges and the external magnetic field. It captures the dynamics of the cloud under its self-Coulomb field, self-magnetic field and an external magnetic field. It is assumed that the electrons move much slower than the speed of light and hence it is not necessary to use retarded fields. Also, electrodynamic radiation is negligible. Under this assumption, the self-magnetic field will be negligible unless the charge density is extremely high.

The increment of time is linear and in Δt step, counted by n as

$$t = (n - 1)\Delta t; \quad n = 1, 2, 3, \dots \quad (A1)$$

At each time instant, the force on the i th electron is

$$\mathbf{F}_i^{(n)} = \frac{e^2}{4\pi\epsilon_0} \sum_{j \neq i}^N \frac{\mathbf{r}_i^{(n)} - \mathbf{r}_j^{(n)}}{|\mathbf{r}_i^{(n)} - \mathbf{r}_j^{(n)}|^3} - e\mathbf{v}_i^{(n)} \times \left\{ \mathbf{B} - e \frac{\mu_0}{4\pi} \sum_{j \neq i}^N \mathbf{v}_j^{(n)} \times \frac{\mathbf{r}_i^{(n)} - \mathbf{r}_j^{(n)}}{|\mathbf{r}_i^{(n)} - \mathbf{r}_j^{(n)}|^3} \right\}, \quad (A2)$$

where $\mathbf{r}_i^{(n)}$ and $\mathbf{v}_i^{(n)}$ are the position and velocity of the i th electron at n th time step, respectively. At the initial time when $n = 1$, the position and the velocity of the electrons can have any distribution, which is generated by a random process. \mathbf{B} is the external magnetic field and the term next to it in the curly bracket stands for the self-magnetic field and is valid only for sub-relativistic electron velocities. The equation of motion gives

$$\frac{d\mathbf{p}_i^{(n)}}{dt} = \mathbf{F}_i^{(n)}, \quad (A3)$$

where $\mathbf{p}_i^{(n)}$ the momentum of the i th electron at n th time step. Assuming non-relativistic electrons, the velocity and position of the i th electron at the next time step will be

$$\mathbf{v}_i^{(n+1)} = \mathbf{v}_i^{(n)} + \frac{\mathbf{F}_i^{(n)}}{m} \Delta t \quad ; \quad \mathbf{r}_i^{(n+1)} = \mathbf{r}_i^{(n)} + \mathbf{v}_i^{(n)} \Delta t, \quad (A4)$$

respectively, which will be used to calculate $\mathbf{F}_i^{(n+1)}$. The iteration continuous till the end time of the simulation. Time step is selected as the smallest value where any further reduction does not increase the accuracy of the simulation considerably.

Appendix B: Generalization of current density method

Suppose we have a spherically symmetric charge distribution of the following form

$$\rho(R, t) = -Ne \frac{f(R, \sigma_R(t))}{\frac{4}{3}\pi\sigma_R^3(t)}, \quad (B1)$$

where $f(R, \sigma_R(t))$ is a unitless function, the integral of which over the whole space equals one. Let us define a current density as

$$\mathbf{J} = \frac{\dot{\sigma}_R}{\sigma_R} R \rho(R, t) \hat{\mathbf{R}}. \quad (B2)$$

The goal is to use the continuity equation $\nabla \cdot \mathbf{J} = -\frac{\partial}{\partial t} \rho(R, t)$ to see under which conditions the definition in Eq. (B2) holds. The time-derivative of the charge density in Eq. (B1) is

$$\frac{\partial}{\partial t} \rho(R, t) = Ne \frac{3\dot{\sigma}_R f(R, \sigma_R(t))}{\frac{4}{3}\pi\sigma_R^4(t)} - \frac{Ne}{\frac{4}{3}\pi\sigma_R^3(t)} \frac{\partial f(R, \sigma_R(t))}{\partial t}. \quad (B3)$$

The divergence of the current density in Eq. (B2) is

$$\begin{aligned} \nabla \cdot \mathbf{J} &= \frac{\dot{\sigma}_R}{\sigma_R} \frac{1}{R^2} \frac{\partial}{\partial R} (R^3 \rho(R, t)) = \frac{\dot{\sigma}_R}{\sigma_R} \frac{1}{R^2} \left(3R^2 \rho(R, t) + R^3 \frac{\partial}{\partial R} \rho(R, t) \right) \\ &= -Ne \frac{\dot{\sigma}_R}{\sigma_R} \left(3 \frac{f(R, \sigma_R(t))}{\frac{4}{3}\pi\sigma_R^3(t)} + \frac{R}{\frac{4}{3}\pi\sigma_R^3(t)} \frac{\partial}{\partial R} f(R, \sigma_R(t)) \right). \end{aligned} \quad (B4)$$

For the continuity equation to hold we equate Eq. (B3) to the negative of Eq. (B4) and get

$$\frac{\partial f(R, \sigma_R(t))}{\partial t} = -\frac{\dot{\sigma}_R}{\sigma_R} R \frac{\partial}{\partial R} f(R, \sigma_R(t)). \quad (B5)$$

The left-hand-side of Eq. (B5) can be rewritten as

$$\frac{\partial f(R, \sigma_R(t))}{\partial t} = \frac{\partial f(R, \sigma_R(t))}{\partial \sigma_R(t)} \dot{\sigma}_R, \quad (B6)$$

which simplifies Eq. (B5) to

$$\sigma_R \frac{\partial f(R, \sigma_R(t))}{\partial \sigma_R(t)} = -R \frac{\partial}{\partial R} f(R, \sigma_R(t)). \quad (B7)$$

Eq. (B7) demands that

$$f(R, \sigma_R(t)) = f\left(\frac{R}{\sigma_R(t)}\right), \quad (B8)$$

because if we evaluate terms $\frac{\partial}{\partial R} f\left(\frac{R}{\sigma_R(t)}\right)$ and $\frac{\partial}{\partial \sigma_R(t)} f\left(\frac{R}{\sigma_R(t)}\right)$, we will have

$$\frac{\partial}{\partial R} f\left(\frac{R}{\sigma_R(t)}\right) = \frac{df}{d\left(\frac{R}{\sigma_R(t)}\right)} \frac{\partial}{\partial R} \left(\frac{R}{\sigma_R(t)}\right) = \frac{df}{d\left(\frac{R}{\sigma_R(t)}\right)} \frac{1}{\sigma_R(t)} \quad (B9)$$

and

$$\frac{\partial}{\partial \sigma_R(t)} f\left(\frac{R}{\sigma_R(t)}\right) = \frac{df}{d\left(\frac{R}{\sigma_R(t)}\right)} \frac{\partial}{\partial \sigma_R(t)} \left(\frac{R}{\sigma_R(t)}\right) = \frac{df}{d\left(\frac{R}{\sigma_R(t)}\right)} \frac{-R}{\sigma_R^2(t)}, \quad (B10)$$

which satisfy Eq (B7). In words, any distribution in the form of

$$\rho(R, t) = \frac{f\left(\frac{R}{\sigma_R(t)}\right)}{\frac{4}{3}\pi\sigma_R^3(t)} \quad (B11)$$

have a corresponding current density in Eq. (B2).

Appendix C: General treatment of Coulomb explosion of spherically symmetric charge distributions

For the general charge case of a spherically symmetric distribution $\rho(R, t)$, we use the Gauss's law to find the current density in terms of the charge density

$$J(R, t) = -\frac{\hat{\mathbf{R}}}{R^2} \frac{\partial}{\partial t} \int_0^R \rho(R', t) R'^2 dR'. \quad (C1)$$

The corresponding drift velocity is

$$\nu = \frac{J(R, t)}{\rho(R, t)} = - \frac{\frac{\partial}{\partial t} \int_0^R R'^2 \rho(R', t) dR'}{R^2 \rho(R, t)} \hat{R}. \quad (C2)$$

Now, we find the material derivative of the drift velocity given by Eq. (13) by calculating terms $\partial v / \partial t$ and $v \cdot \nabla v$. We have

$$\frac{\partial \mathbf{v}}{\partial t} = -\hat{\mathbf{R}} \frac{\rho(R, t) \frac{\partial^2}{\partial t^2} \int_0^R R'^2 \rho(R', t) dR' - \frac{\partial}{\partial t} \rho(R, t) \frac{\partial}{\partial t} \int_0^R R'^2 \rho(R', t) dR'}{R^2 \rho^2(R, t)}, \quad (C3)$$

and

$$\boldsymbol{v} \cdot \nabla \boldsymbol{v} = \hat{\boldsymbol{R}} \boldsymbol{v} \frac{\partial \boldsymbol{v}}{\partial R} = \hat{\boldsymbol{R}} \frac{\frac{\partial}{\partial t} \int_0^R R'^2 \rho(R', t) dR'}{R^2 \rho(R, t)} \frac{\partial}{\partial R} \frac{\frac{\partial}{\partial t} \int_0^R R'^2 \rho(R', t) dR'}{R^2 \rho(R, t)}. \quad (C4)$$

Evaluation of the spatial derivative on the right-hand-side of Eq. (C4) gives

$$\mathbf{v} \cdot \nabla \mathbf{v} = \hat{\mathbf{R}} \frac{\frac{\partial}{\partial t} \int_0^R R'^2 \rho(R', t) dR'}{R^2 \rho(R, t)} \left\{ \frac{R^2 \rho(R, t) \frac{\partial}{\partial t} R^2 \rho(R, t) - \left(2R\rho(R, t) + R^2 \frac{\partial}{\partial R} \rho(R, t) \right) \frac{\partial}{\partial t} \int_0^R R'^2 \rho(R', t) dR'}{R^4 \rho^2(R, t)} \right\}. \quad (C5)$$

Adding the Eq. (C3) and (C5) will give the material derivative of the drift velocity as

$$\frac{d\mathbf{v}}{dt} = \frac{\partial \mathbf{v}}{\partial t} + \mathbf{v} \cdot \nabla \mathbf{v} = -\hat{\mathbf{R}} \frac{\rho(R, t) \frac{\partial^2}{\partial t^2} \int_0^R R'^2 \rho(R', t) dR' - 2 \frac{\partial}{\partial t} \rho(R, t) \frac{\partial}{\partial t} \int_0^R R'^2 \rho(R', t) dR'}{R^2 \rho^2(R, t)} - \hat{\mathbf{R}} \left[\frac{2}{R^5 \rho^2(R, t)} + \frac{\frac{\partial}{\partial R} \rho(R, t)}{R^4 \rho^3(R, t)} \right] \left(\frac{\partial}{\partial t} \int_0^R R'^2 \rho(R', t) dR' \right)^2. \quad (C6)$$

By use of the Gauss's law, we find the electric field of the charge distribution as

$$\mathbf{E}(R, t) = \frac{1}{\epsilon_0 R^2} \int_0^R \rho(R', t) R'^2 dR'. \quad (C7)$$

The non-relativistic equation of motion

$$\frac{d\mathbf{v}}{dt} = -\frac{e}{m} \mathbf{E}(R, t) \quad (C8)$$

after some algebraic simplifications gives

$$\left[-\rho(R, t) \frac{\partial^2}{\partial t^2} + 2 \frac{\partial \rho(R, t)}{\partial t} \frac{\partial}{\partial t} + \frac{e}{\epsilon_0} \rho^2(R, t) \right] \int_0^R R'^2 \rho(R', t) dR' = \left[\frac{2}{R^3} + \frac{1}{R^2 \rho(R, t)} \frac{\partial \rho(R, t)}{\partial R} \right] \left(\frac{\partial}{\partial t} \int_0^R R'^2 \rho(R', t) dR' \right)^2, \quad (C9)$$

which is a non-linear integrodifferential equation containing only $\rho(R, t)$. The equation, though difficult to deal with, has an advantage of determining the charge density as a function of both R and t and hence can fully determine the dynamics of the distribution. Generalization to the relativistic expansion is tedious but straightforward. The method can be applied to charge distribution of cylindrical symmetry in a uniform magnetic field as well.

References

- [1] Zandi, Omid, Allan E. Sykes, Ryan D. Cornelius, Frank M. Alcorn, Brandon Zerbe, Phillip M. Duxbury, Bryan W. Reed, and Renske M. van der Veen. "Transient lensing from a photoemitted electron gas imaged by ultrafast electron microscopy." arXiv preprint arXiv:2001.01389 (2020).
- [2] Boyer, K., T. S. Luk, J. C. Solem, and C. K. Rhodes. "Kinetic energy distributions of ionic fragments produced by subpicosecond multiphoton ionization of N 2." Physical Review A 39, no. 3 (1989): 1186.
- [3] Last, Isidore, Israel Schek, and Joshua Jortner. "Energetics and dynamics of Coulomb explosion of highly charged clusters." The Journal of chemical physics 107, no. 17 (1997): 6685-6692.
- [4] Zweiback, J., R. A. Smith, T. E. Cowan, G. Hays, K. B. Wharton, V. P. Yanovsky, and Todd Ditmire. "Nuclear fusion driven by Coulomb explosions of large deuterium clusters." Physical review letters 84, no. 12 (2000): 2634.

- [5] Kaplan, Alexander E., Boris Y. Dubetsky, and P. L. Shkolnikov. "Shock shells in coulomb explosions of nanoclusters." *Physical review letters* 91, no. 14 (2003): 143401.
- [6] Last, Isidore, and Joshua Jortner. "Electron and nuclear dynamics of molecular clusters in ultraintense laser fields. III. Coulomb explosion of deuterium clusters." *The Journal of chemical physics* 121.7 (2004): 3030-3043.
- [7] Sakabe, S., S. Shimizu, M. Hashida, F. Sato, T. Tsuyukushi, K. Nishihara, S. Okihara et al. "Generation of high-energy protons from the Coulomb explosion of hydrogen clusters by intense femtosecond laser pulses." *Physical Review A* 69, no. 2 (2004): 023203.
- [8] Döppner, Th, Th Fennel, Th Diederich, J. Tiggesbäumer, and K. H. Meiwes-Broer. "Controlling the Coulomb explosion of silver clusters by femtosecond dual-pulse laser excitation." *Physical review letters* 94, no. 1 (2005): 013401.
- [9] Kovalev, V. F., K. I. Popov, V. Yu Bychenkov, and W. Rozmus. "Laser triggered Coulomb explosion of nanoscale symmetric targets." *Physics of plasmas* 14, no. 5 (2007): 053103.
- [10] Hashida, M., H. Mishima, S. Tokita, and S. Sakabe. "Non-thermal ablation of expanded polytetrafluoroethylene with an intense femtosecond-pulse laser." *Optics express* 17, no. 15 (2009): 13116-13121.
- [11] Mirza, Inam, Nadezhda M. Bulgakova, Jan Tomáštík, Václav Michálek, Ondřej Haderka, Ladislav Fekete, and Tomáš Mocek. "Ultrashort pulse laser ablation of dielectrics: Thresholds, mechanisms, role of breakdown." *Scientific reports* 6 (2016): 39133.
- [12] Mason, Philip E., Frank Uhlig, Václav Vaněk, Tillmann Buttersack, Sigurd Bauerecker, and Pavel Jungwirth. "Coulomb explosion during the early stages of the reaction of alkali metals with water." *Nature chemistry* 7, no. 3 (2015): 250.
- [13] Vager, Z., R. Naaman, and E. P. Kanter. "Coulomb explosion imaging of small molecules." *Science* 244, no. 4903 (1989): 426-431.]
- [14] Pitzer, Martin, Maksim Kunitski, Allan S. Johnson, Till Jahnke, Hendrik Sann, Felix Sturm, Lothar Ph H. Schmidt et al. "Direct determination of absolute molecular stereochemistry in gas phase by Coulomb explosion imaging." *Science* 341, no. 6150 (2013): 1096-1100.
- [15] Ablikim, Utuq, Cédric Bomme, Hui Xiong, Evgeny Savelyev, Razib Obaid, Balram Kaderiya, Sven Augustin et al. "Identification of absolute geometries of cis and trans molecular isomers by Coulomb Explosion Imaging." *Scientific reports* 6 (2016): 38202.
- [16] Serafini, Luca. "The short bunch blow-out regime in RF photoinjectors." In *AIP Conference Proceedings*, vol. 413, no. 1, pp. 321-334. American Institute of Physics, 1997.
- [17] Passlack, S., S. Mathias, O. Andreyev, D. Mitnacht, M. Aeschlimann, and M. Bauer. "Space charge effects in photoemission with a low repetition, high intensity femtosecond laser source." *Journal of applied physics* 100, no. 2 (2006): 024912.

[18] Geoffroy, Ghita, Guillaume Duchateau, Nikita Fedorov, Patrick Martin, and Stéphane Guizard. "Influence of electron Coulomb explosion on photoelectron spectra of dielectrics irradiated by femtosecond laser pulses." *Laser Physics* 24, no. 8 (2014): 086101.

[19] Bach, Nora, Till Domröse, Armin Feist, Thomas Rittmann, Stefanie Strauch, Claus Ropers, and Sascha Schäfer. "Coulomb interactions in high-coherence femtosecond electron pulses from tip emitters." *Structural Dynamics* 6, no. 1 (2019): 014301.

[20] Ramo, Simon. "Space charge and field waves in an electron beam." *Physical Review* 56, no. 3 (1939): 276.

[21] Kapchinskij, I. M., and V. V. Vladimirkij. "Limitations of proton beam current in a strong focusing linear accelerator associated with the beam space charge." (1959): 274-287.

[22] Sacherer, Frank J. "RMS envelope equations with space charge." *IEEE Transactions on Nuclear Science* 18, no. 3 (1971): 1105-1107.

[23] Michalik, A. M., and J. E. Sipe. "Analytic model of electron pulse propagation in ultrafast electron diffraction experiments." *Journal of applied physics* 99, no. 5 (2006): 054908.

[24] Reed, Bryan W. "Femtosecond electron pulse propagation for ultrafast electron diffraction." *Journal of applied physics* 100, no. 3 (2006): 034916.

[25] Tao, Zhensheng, He Zhang, P. M. Duxbury, Martin Berz, and Chong-Yu Ruan. "Space charge effects in ultrafast electron diffraction and imaging." *Journal of Applied Physics* 111, no. 4 (2012): 044316.

[26] Zerbe, B. S., Xukun Xiang, C-Y. Ruan, S. M. Lund, and P. M. Duxbury. "Dynamical bunching and density peaks in expanding Coulomb clouds." *Physical Review Accelerators and Beams* 21, no. 6 (2018): 064201.

[27] Monastyrski, M. A., V. P. Degtyareva, M. Ya Schelev, and V. A. Tarasov. "Dynamics of electron bunches in subpicosecond streak tubes." *Nuclear Instruments and Methods in Physics Research Section A: Accelerators, Spectrometers, Detectors and Associated Equipment* 427, no. 1-2 (1999): 225-229.

[28] Pierce, J. R. "The wave picture of microwave tubes." *Bell System Technical Journal* 33, no. 6 (1954): 1343-1372.

[29] Li, Bin, Zhong Hai Yang, Jian Qing Li, Xiao Fang Zhu, Tao Huang, Quan Hu, Yu Lu Hu et al. "Theory and design of microwave-tube simulator suite." *IEEE Transactions on Electron Devices* 56, no. 5 (2009): 919-927.

[30] Sarid, E., F. Anderegg, and C. F. Driscoll. "Cyclotron resonance phenomena in a non-neutral multispecies ion plasma." *Physics of Plasmas* 2, no. 8 (1995): 2895-2907.

[31] Wang, Tao-Chin Lin, and Alan G. Marshall. "Coulomb broadening in Fourier transform ion cyclotron resonance mass spectrometry." *International journal of mass spectrometry and ion processes* 68, no. 3 (1986): 287-301.

- [32] Gould, Roy W., and Michael A. LaPointe. "Cyclotron resonance in a pure electron plasma column." *Physical review letters* 67, no. 26 (1991): 3685.
- [33] Prasad, S. A., G. J. Morales, and B. D. Fried. "Cyclotron resonance phenomena in a non-neutral plasma." *The Physics of fluids* 30, no. 10 (1987): 3093-3105.
- [34] Thompson, James K., Simon Rainville, and David E. Pritchard. "Cyclotron frequency shifts arising from polarization forces." *Nature* 430, no. 6995 (2004): 58-61.
- [35] Jeffries, J. B., S. E. Barlow, and G. H. Dunn. "Theory of space-charge shift of ion cyclotron resonance frequencies." *International Journal of Mass Spectrometry and Ion Processes* 54, no. 1-2 (1983): 169-187.
- [36] Affolter, M., F. Anderegg, and C. F. Driscoll. "Space Charge Frequency Shifts of the Cyclotron Modes in Multi-Species Ion Plasmas." *Journal of The American Society for Mass Spectrometry* 26, no. 2 (2014): 330-336.
- [37] Fujita, S., and A. Lodder. "On the cyclotron resonance width due to the electron-charged impurity interaction." *Physica B+C* 83, no. 2 (1976): 117-128.
- [38] Kawamura, Hajimu, Haruo Saji, Masakazu Fukai, Kenji Sekido, and Isamu Imai. "Cyclotron resonance line broadening due to carrier-carrier interaction in germanium." *Journal of the Physical Society of Japan* 19, no. 3 (1964): 288-296.
- [39] Kallin, C., and Bertrand I. Halperin. "Many-body effects on the cyclotron resonance in a two-dimensional electron gas." *Physical Review B* 31, no. 6 (1985): 3635.
- [40] Maag, Thomas, Andreas Bayer, Sebastian Baierl, Matthias Hohenleutner, Tobias Korn, Christian Schüller, Dieter Schuh et al. "Coherent cyclotron motion beyond Kohn's theorem." *Nature Physics* 12, no. 2 (2016): 119-123.
- [41] Fujita, S., and M. Prasad. "Theory of cyclotron resonance lineshape for an electron-impurity system in two dimensions." *Journal of Physics and Chemistry of Solids* 38, no. 12 (1977): 1351-1353.
- [42] Bisti, V. E., and N. N. Kirova. "Coulomb interaction and electron-hole asymmetry in cyclotron resonance of bilayer graphene in a high magnetic field." *Physical Review B* 84, no. 15 (2011): 155434.
- [43] Tonks, Lewi. "Theory of magnetic effects in the plasma of an arc." *Physical Review* 56, no. 4 (1939): 360.
- [44] Forrest, J. R., and R. N. Franklin. "The diamagnetism of a plasma column." *Proceedings of the Royal Society of London. Series A. Mathematical and Physical Sciences* 305, no. 1481 (1968): 251-257.
- [45] Hazeltine, Richard D. *The framework of plasma physics*. CRC Press, 2004, pp. 64-65.
- [46] Young, W. C., A. B. Hassam, C. A. Romero-Talamás, R. F. Ellis, and C. Teodorescu. "Diamagnetism of rotating plasma." *Physics of Plasmas* 18, no. 11 (2011): 112505.
- [47] Kohn, Walter. "Cyclotron resonance and de Haas-van Alphen oscillations of an interacting electron gas." *Physical Review* 123, no. 4 (1961): 1242.

- [48] McBride, Vanessa A., J. Wilms, M. J. Coe, I. Kreykenbohm, R. E. Rothschild, W. Coburn, J. L. Galache, P. Kretschmar, W. R. T. Edge, and R. Staubert. "Study of the cyclotron feature in MXB 0656-072." *Astronomy & Astrophysics* 451, no. 1 (2006): 267-272.
- [49] Nishimura, Osamu. "Formation mechanism for broad and shallow profiles of cyclotron lines in accreting X-ray pulsars." *The Astrophysical Journal* 672, no. 2 (2008): 1127.
- [50] Staubert, R., J. Trümper, E. Kendziorra, D. Klochkov, K. Postnov, P. Kretschmar, K. Pottschmidt et al. "Cyclotron lines in highly magnetized neutron stars." *Astronomy & Astrophysics* 622 (2019): A61.